Author(s): D'Angelo, Stefano

Title: Generalized Moog Ladder Filter: Part II Explicit Nonlinear Model through a Novel Delay-Free Loop Implementation Method

Year: 2014

Version: Post print / Accepted author version

Please cite the original version:

S. D Angelo and V. Välimäki. Generalized Moog Ladder Filter: Part II Explicit Nonlinear Model through a Novel Delay-Free Loop Implementation Method. IEEE Trans. Audio, Speech, and Lang. Process., vol. 22, no. 12, pp. 1873 1883, December 2014.

Generalized Moog Ladder Filter: Part II – Explicit Nonlinear Model through a Novel Delay-Free Loop Implementation Method

Stefano D'Angelo and Vesa Välimäki, *Senior Member, IEEE*

***Abstract*—One of the most critical aspects of virtual analog simulation of circuits for music production consists in accurate reproduction of their nonlinear behavior, yet this goal is in many cases difficult to achieve due to the presence of implicit differential equations in circuit models, since they naturally map to delay-free loops in the digital domain. This paper presents a novel and general method for non-iteratively implementing these loops in such a way that the linear response around a chosen operating point is preserved, the topology is minimally affected, and transformation of nonlinearities is not required. This technique is then applied to a generalized model of the Moog ladder filter, resulting in an implementation that outperforms its predecessors with only a modest computational load penalty. This digital version of the filter is shown to offer strong stability guarantees w.r.t. parameter variation, allows the extraction of different frequency response modes by simple mixing of individual ladder stage outputs, and is suitable for real-time sound synthesis and audio effects processing.**

***Index Terms*—Acoustic signal processing, circuit simulation, IIR filters, music, resonator filters.**

I. Introduction

THE Moog ladder filter [1], [2] owes much of its popularity to the "warmth" in the sound it produces. This distinctive tonal quality is determined by the nonlinear side effects introduced by the transistors in the filter circuit. This is often the case in musical analog circuits, and indeed faithful emulation of nonlinear circuit behavior is a fundamental topic in virtual analog modeling [3]–[5].

While the first part of this work [6] studied a generalized version of the filter having an arbitrary number of ladder stages, with special emphasis on parameterization strategies, the purpose of this paper is to define a non-iterative digital implementation that retains the linear response of the simulated system and, at the same time, mimics its nonlinear behavior.

The difficulty in reaching such a goal is testified by several studies dedicated to the original filter [7]–[10]. In particular, the presence of implicit nonlinear differential equations in the large-signal model of the circuit, and for which no analytical solution is known, represents the major obstacle towards the development of a realistic non-iterative digital model, since such equations naturally translate to non-directly-computable delay-free loops in the digital domain. Several techniques to overcome this specific problem have been proposed in the literature, yet they are limited to linear systems [11], [12], propose iterative solutions [13]–[16], or require nontrivial transformation of filter topology and/or nonlinear elements [17]–[20].

This work tackles this issue by defining a novel and general method to implement delay-free loops in nonlinear filters through different kinds of relatively simple linear compensation strategies and is organized as follows. Section II summarizes some of the results discussed in [6] that are preparatory to the discussion and defines an implicit discretization of the system. Section III presents the aforementioned delay-free implementation method. Section IV derives the explicit digital model of the circuit. Section V evaluates the proposed implementation and compares it to those developed in [7] and [10], as well as with a SPICE simulation [21] of the circuit. The paper eventually concludes with Section VI.

II. Generalized Moog Ladder Filter Circuit

The generalized Moog ladder filter circuit [1], [2] is depicted in Fig. 1. This circuit consists of a differential amplifier transistor pair, driven by the externally-controlled current source I_{ctl}, and of a series of N consecutive and buffered low-pass stages. The filter output is extracted from the last stage and fed back into the input differential amplifier through a subcircuit that functionally implements phase-inversion and amplification of the signal by a user-controllable feedback gain loop parameter k. It is shown in [6] that a valid large-signal model for any positive number N of ladder stages is given by

$$\frac{\mathrm{d}\Delta V_i}{\mathrm{d}t} = \frac{I_{\mathrm{ctl}}}{2C}\left[\tanh\left(\frac{\Delta V_{i-1}}{2V_{\mathrm{T}}}\right) - \tanh\left(\frac{\Delta V_i}{2V_{\mathrm{T}}}\right)\right], \quad (1)$$

for $i > 1$, while

$$\frac{\mathrm{d}\Delta V_1}{\mathrm{d}t} = -\frac{I_{\mathrm{ctl}}}{2C}\left[\tanh\left(\frac{\Delta V_1}{2V_{\mathrm{T}}}\right) + \tanh\left(\frac{V_{\mathrm{in}} + k\Delta V_N}{2V_{\mathrm{T}}}\right)\right], \quad (2)$$

where ΔV_i represents the voltage across the capacitor in each stage $i \in [1, N]$, I_{ctl} is the control current, V_{in} is the input voltage, k is the feedback coefficient, C is the capacitance value of each capacitor (assuming them to be all equivalent), and V_{T} is the thermal voltage ($\approx 26\,\mathrm{mV}$ at room temperature $300\,\mathrm{K}$).

Manuscript received January 17, 2014, revised May 02, 2014, revised August 07, 2014.

S. D'Angelo is with the Department of Signal Processing and Acoustics, Aalto University, School of Electrical Engineering, P.O. Box 13000, FI-00076 AALTO, Espoo, Finland (email: stefano.d'angelo@aalto.fi).

S. D'Angelo's research is funded by the GETA Graduate School in Electronics, Telecommunications and Automation, and by the Aalto ELEC Doctoral School.

V. Välimäki is with the Department of Signal Processing and Acoustics, Aalto University, School of Electrical Engineering (email: vesa.valimaki@aalto.fi).

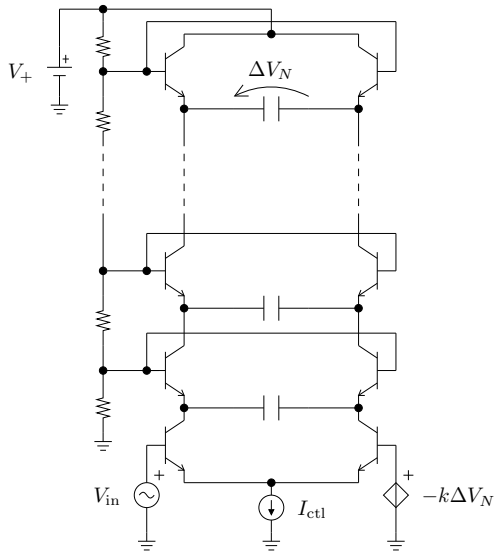

Fig. 1. Generalized ladder filter circuit having N stages.

The behavior of the circuit in its linear region of operation is then studied, for any positive value of N, by considering that when a null input signal $V_{\text{in}} = 0$ is applied to the system, the derivatives in (1) and (2) are null, and hence $\Delta V_N = \Delta V_{N-1} = ... = \Delta V_1 = -k\Delta V_N \Rightarrow \Delta V_i = 0$ is the operating point of each stage. It is therefore possible to linearize $\tanh(x) \approx x$ around $x_0 = 0$, leading to

$$\frac{\Delta V_i(s)}{\Delta V_{i-1}(s)} = -\frac{\Delta V_1(s)}{V_{\text{in}}(s) + k\Delta V_N(s)} = \frac{\frac{I_{\text{ctl}}}{4CV_{\text{T}}}}{s + \frac{I_{\text{ctl}}}{4CV_{\text{T}}}}, \quad (3)$$

for $i \geq 2$.

When $N = 1$, obtaining the cut-off frequency of the filter $f_{\text{c}} = \frac{I_{\text{ctl}}}{8\pi CV_{\text{T}}}(1 + k)$ is trivial, while in all other cases the cut-off frequency of the leading poles of the system $f_{\text{c}} = \frac{I_{\text{ctl}}}{8\pi CV_{\text{T}}} A_0(k)$, where $A_0(k) = \sqrt{1 + \sqrt[N/2]{k} - 2\sqrt[N]{k}\cos\left(\frac{\pi}{N}\right)}$. It is also possible to define a *natural cut-off frequency* $\widehat{f}_{\text{c}} \triangleq f_{\text{c}}|_{k=0} = \frac{I_{\text{ctl}}}{8\pi CV_{\text{T}}}$, that stands in linear proportion to I_{ctl}. For $N = 1$, $\widehat{f}_{\text{c}} = \frac{f_{\text{c}}}{1+k}$, and otherwise $\widehat{f}_{\text{c}} = \frac{f_{\text{c}}}{A_0(k)}$. The quantity

$$\alpha(k) \triangleq \begin{cases} 1 + k, & \text{when } N = 1, \\ A_0(k), & \text{when } N > 1, \end{cases} \quad (4)$$

is introduced for convenience, so that $f_{\text{c}} = \frac{I_{\text{ctl}}}{8\pi CV_{\text{T}}}\alpha(k)$ and $\widehat{f}_{\text{c}} = \frac{f_{\text{c}}}{\alpha(k)}$ for any N.

A. Implicit Discretization

By discretizing the derivative in (1) with a bilinear-transformed derivator with pre-warping around a given frequency f_{w} and then solving for $\Delta V_i[n]$, one gets

$$\begin{aligned}\Delta V_i[n] =& \Delta V_i[n-1] + 2V_{\text{T}}g \\ &\left[\tanh\left(\frac{\Delta V_{i-1}[n]}{2V_{\text{T}}}\right) + \tanh\left(\frac{\Delta V_{i-1}[n-1]}{2V_{\text{T}}}\right)\right. \\ &\left. - \tanh\left(\frac{\Delta V_i[n]}{2V_{\text{T}}}\right) - \tanh\left(\frac{\Delta V_i[n-1]}{2V_{\text{T}}}\right)\right], \end{aligned} \quad (5)$$

with

$$g = \frac{\tan\left(\pi\frac{f_{\text{w}}}{f_{\text{s}}}\right)}{f_{\text{w}}}\frac{I_{\text{ctl}}}{8\pi CV_{\text{T}}} = \frac{\tan\left(\pi\frac{f_{\text{w}}}{f_{\text{s}}}\right)}{f_{\text{w}}}\widehat{f}_{\text{c}}, \quad (6)$$

and similarly for (2),

$$\begin{aligned}\Delta V_1[n] =& \Delta V_1[n-1] - 2V_{\text{T}}g \\ &\left[\tanh\left(\frac{\Delta V_1[n]}{2V_{\text{T}}}\right) + \tanh\left(\frac{\Delta V_1[n-1]}{2V_{\text{T}}}\right)\right. \\ &\left. + \tanh\left(\frac{V_{\text{u}}[n]}{2V_{\text{T}}}\right) + \tanh\left(\frac{V_{\text{u}}[n-1]}{2V_{\text{T}}}\right)\right], \end{aligned} \quad (7)$$

with $V_{\text{u}}[n] = V_{\text{in}}[n] + k\Delta V_N[n]$.

A direct implementation of such an implicitly-defined system would require, for each input sample, the evaluation of one implicit loop for each of the N stages plus one global loop that itself includes all N ladder stage loops. While iterative approaches have been successfully applied for discretizing a similar circuit [22]–[24], the rest of this paper will concentrate on defining an analogous explicit discrete-time system that retains much of the linear and nonlinear behavior of the analog system.

III. Implementation of Delay-Free Loops

As already discussed, deriving a non-iterative and computable discretization of the model described by (1) and (2) is nontrivial due to the presence of nonlinearities involving instantaneous feedbacks in each stage and through the global feedback path. Recent attempts to develop such a model [7], [10] add fictitious unit delays to resolve this problem, thus compromising the linear response of the resulting digital filter around its operating point and therefore requiring ad-hoc parameter compensation strategies. Furthermore, [25] discusses the possibility of obtaining different frequency response modes (e.g., high-pass, band-pass, notch) through simple mixing of the outputs of individual ladder stages, hence making it desirable for a digital model to be able to provide such outputs.

This section, therefore, introduces a novel and general method for implementing delay-free loops non-iteratively in such a way that the linear response of a system is preserved around a static operating point, as is its topology to a certain degree, and such that nonlinearities do not need to be transformed. Since the operating point is chosen beforehand and does not vary during the operation of the resulting system, this cannot be regarded as an adaptive technique.

A. Problem Statement

The systems of interest are causal time-invariant single-input single-output discrete-time filters. Any such system can be described by the equation

$$y[n] = f(x[n], y[n]), \quad (8)$$

where $x[n]$ is the input signal, $y[n]$ is the output signal, and $f()$ is a causal mapping operator whose domain includes all potential points $(x[n], y[n])$. Fig. 2(a) shows a block diagram representation of such a filter. Note that the above definition

allows $f()$ to include memory effects and to depend "instantaneously" on $y[n]$, thus potentially resulting in an implicit equation that corresponds to a delay-free loop.

Finding an explicit solution, in such cases, can often be impossible, or otherwise regarded as undesirable, inappropriate, or inconvenient. Inserting a fictitious delay unit in the feedback branch represents the simplest possible modification to the system that provides a non-iterative approximation, yet generally compromising its linear response. The technique introduced hereafter essentially improves this basic method by also adding linear compensation filters in all signal paths so that the linear response of the system is preserved around a fixed working point (x_0, y_0), near which it may be possible to linearize $f(x[n], y[n]) \approx v[n] + w[n] + c$, where $v[n] = \sum_{i=0}^{B} b_i x[n-i] + \sum_{i=1}^{E} e_i v[n-i]$, and $w[n] = \sum_{i=0}^{A} a_i y[n-i] + \sum_{i=1}^{D} d_i w[n-i]$. This particular linearization strategy allows to conveniently represent IIR-type approximations with a finite number of coefficients, a property which will prove to be useful later on. The linearized filter is therefore represented in the z domain by

$$Y(z) \approx \frac{1-\sum_{i=1}^{D} d_i z^{-i}}{1-\sum_{i=1}^{E} e_i z^{-i}} \frac{X(z)\sum_{i=0}^{B} b_i z^{-i} + c\frac{z^{-1}}{1-z^{-1}}\left(1-\sum_{i=1}^{E} e_i z^{-i}\right)}{1-\sum_{i=1}^{D} d_i z^{-i} - \sum_{i=0}^{A} a_i z^{-i}}. \tag{9}$$

Applying the same approximation to the analogous filter described by

$$\widehat{y}[n] = h_{\mathrm{ff}}[n] * \left(f\left(h_{\mathrm{in}}[n] * x[n], h_{\mathrm{fb}}[n] * \widehat{y}[n-1]\right) + \widehat{c}[n]\right), \tag{10}$$

and depicted in Fig. 2(b), where $*$ denotes convolution, and $h_{\mathrm{in}}[n]$, $h_{\mathrm{ff}}[n]$, and $h_{\mathrm{fb}}[n]$ are the discrete-time-domain impulse responses of $H_{\mathrm{in}}(z)$, $H_{\mathrm{ff}}(z)$, and $H_{\mathrm{fb}}(z)$, respectively, results in

$$\widehat{Y}(z) \approx \frac{H_{\mathrm{ff}}(z)\left(1-\sum_{i=1}^{D} d_i z^{-i}\right)}{1-\sum_{i=1}^{E} e_i z^{-i}} \frac{X(z)H_{\mathrm{in}}(z)\sum_{i=0}^{B} b_i z^{-i} + K(z)(1-\sum_{i=1}^{E} e_i z^{-i})}{1-\sum_{i=1}^{D} d_i z^{-i} - z^{-1}H_{\mathrm{fb}}(z)H_{\mathrm{ff}}(z)\sum_{i=0}^{A} a_i z^{-i}}, \tag{11}$$

with $K(z) = c\frac{z^{-1}}{1-z^{-1}} + \widehat{C}(z)$. This second filter (10) is always directly computable, unlike the previous one, given that $f()$ is defined over the set of potential argument values.

Both filters can be seen as dual-input single-output LTI systems. Therefore, by the superposition principle, equating (9) and (11), imposing $X(z) = 0$, and solving for $\widehat{C}(z)$ leads to

$$\widehat{C}(z) = c\frac{z^{-1}}{1-z^{-1}} \left[\frac{\frac{1-\sum_{i=1}^{D} d_i z^{-i}}{H_{\mathrm{ff}}(z)} - z^{-1}H_{\mathrm{fb}}(z)\sum_{i=0}^{A} a_i z^{-i}}{1-\sum_{i=1}^{D} d_i z^{-i} - \sum_{i=0}^{A} a_i z^{-i}} - 1\right], \tag{12}$$

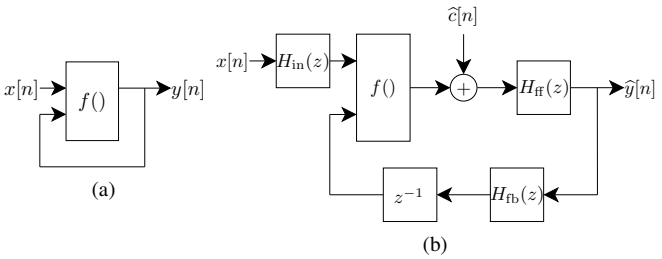

Fig. 2. Block diagram representations of (a) the original implicitly-defined system (8) and (b) the analogous explicitly-defined system (10).

which in turn implies that for the other input it must be

$$\frac{1}{1-\sum_{i=1}^{D} d_i z^{-i} - \sum_{i=0}^{A} a_i z^{-i}} = \frac{H_{\mathrm{ff}}(z)H_{\mathrm{in}}(z)}{1-\sum_{i=1}^{D} d_i z^{-i} - z^{-1}H_{\mathrm{fb}}(z)H_{\mathrm{ff}}(z)\sum_{i=0}^{A} a_i z^{-i}}. \tag{13}$$

Finally, the proposed method overall consists in replacing a non-computable filter expressed in the form (8) with an analogous computable filter of form (10) such that the frequency response of the original implicitly-defined filter, linearized around a chosen operating point (x_0, y_0), is preserved in the analogous explicitly-defined filter, linearized around the same operating point. This substitution is possible if $f()$ can be linearized around (x_0, y_0) and is defined for all its input values in (10), and when $h_{\mathrm{ff}}[n]$, $h_{\mathrm{fb}}[n]$, $h_{\mathrm{in}}[n]$, and $\widehat{c}[n]$ satisfy (12) and (13).

B. Solutions

Let $H_{\mathrm{ff}}(z) = \frac{\sum_{i=0}^{P} p_i z^{-i}}{1-\sum_{i=1}^{S} s_i z^{-i}}$, $H_{\mathrm{fb}}(z) = \frac{\sum_{i=0}^{Q} q_i z^{-i}}{1-\sum_{i=1}^{T} t_i z^{-i}}$, and $H_{\mathrm{in}}(z) = \frac{\sum_{i=0}^{R} r_i z^{-i}}{1-\sum_{i=1}^{U} u_i z^{-i}}$. Then (13) can be reformulated as

$$\begin{aligned}
&\left[\left(1-\sum_{i=1}^{D} d_i z^{-i}\right)\left(1-\sum_{i=1}^{S} s_i z^{-i}\right)\left(1-\sum_{i=1}^{T} t_i z^{-i}\right) - z^{-1}\sum_{i=0}^{A} a_i z^{-i}\sum_{i=0}^{P} p_i z^{-i}\sum_{i=0}^{Q} q_i z^{-i}\right]\left(1-\sum_{i=1}^{U} u_i z^{-i}\right) \\
&= \left(1-\sum_{i=0}^{A} a_i z^{-i} - \sum_{i=1}^{D} d_i z^{-i}\right)\sum_{i=0}^{P} p_i z^{-i}\sum_{i=0}^{R} r_i z^{-i}\left(1-\sum_{i=1}^{T} t_i z^{-i}\right).
\end{aligned} \tag{14}$$

The problem outlined in the previous subsection now reduces to finding values of coefficients p_i, q_i, r_i, s_i, t_i, and u_i that satisfy this last equation.

It is obvious that an infinite number of solutions exists, and also that it is impossible to find general explicit formulations for coefficient values. Therefore, the rest of this subsection explores a few classes of solutions that exhibit appealing properties, namely the existence of explicit and relatively simple coefficient formulae and the presence of the minimum number of coefficients, in general terms and in each specific class, such that $H_{\mathrm{fb}}(z)$ is not necessarily 0. The specific

derivations of resulting formulae are omitted for the sake of brevity.

1) Feedforward Shaping: If $Q = R = T = U = 0$ in (14), it is possible to choose $P = D$ and $S = \max(A + 1, D)$ to obtain

$$\begin{aligned} p_0 &= \frac{1}{(1-a_0)\,r_0}, \quad p_i = -\frac{d_i}{(1-a_0)\,r_0}, \\ s_i &= \frac{1}{1-a_0}\left(d_i + a_i - \frac{q_0}{r_0}a_{i-1}\right), \end{aligned} \tag{15}$$

where r_0 and q_0 are free parameters. This represents the minimum cost solution such that $H_{\mathrm{in}}(z)$ and $H_{\mathrm{fb}}(z)$ are constant values, and both can be arbitrarily chosen.

2) Feedback Shaping: If $P = R = S = U = 0$ in (14), and $A > 0$ or $D > 0$, it is possible to choose $Q = \max(A, D) - 1$ and $T = A$ to obtain

$$p_0 = \frac{1}{(1-a_0)\,r_0}, \quad q_i = \left(d_{i+1} + \frac{a_{i+1}}{a_0}\right) r_0, \quad t_i = -\frac{a_i}{a_0}, \tag{16}$$

where r_0 is a free parameter. This represents the minimum cost solution such that $H_{\mathrm{in}}(z)$ and $H_{\mathrm{ff}}(z)$ are constant values, one of which can be arbitrarily chosen.

3) FIR-only Solution: Let $P = S = T = U = 0$ in (14). If $A = D = 0$, then it is possible to choose $R = 1$ and $Q = 0$ to obtain

$$p_0 = \frac{1}{(1-a_0)\,r_0}, \quad q_0 = -\frac{(1-a_0)}{a_0} r_1, \tag{17}$$

where r_0 and r_1 are free parameters.

Otherwise, it is convenient to choose $R = A$ and $Q = \max(A, D) - 1$, so that for $A \geq 1$

$$\begin{aligned} p_0 &= \frac{a_A}{(1-a_0)\,r_A}, \quad q_i = \frac{(d_{i+1} + a_{i+1})}{a_A} r_A, \\ r_0 &= \frac{r_A}{a_A}, \quad r_i = \frac{a_i}{a_A} r_A, \end{aligned} \tag{18}$$

where r_A is a free parameter, while for $D > A = 0$

$$p_0 = \frac{1}{(1-a_0)\,r_0}, \quad q_i = d_{i+1} r_0, \tag{19}$$

where r_0 is a free parameter. This represents the minimum cost solution such that $H_{\mathrm{fb}}(z)$, $H_{\mathrm{ff}}(z)$, and $H_{\mathrm{in}}(z)$ are FIR filters.

C. Composition

In the most general case, when a filter of form (8) is part of another such filter, the latter can be described as

$$\begin{cases} (y[n], x_1[n]) = f_{\mathrm{r}}(x[n], y[n], x_1[n], y_1[n]) \\ y_1[n] = f_1(x_1[n], y_1[n]) \end{cases}, \tag{20}$$

where $x[n]$, $y[n]$, $x_1[n]$, and $y_1[n]$ are, respectively, the global input, the global output, the input of the inner filter, and the output of the inner filter, and where $f_1()$ characterizes the inner filter, while $f_{\mathrm{r}}()$ describes both the rest of the global filter and its relationship with the inner filter. While it is certainly possible to apply the discussed technique to the inner filter, the same does not hold true for the rest of the global filter (or, at least, not without a multi-dimensional extension).

In this work, we limit ourselves to the commonly encountered case in which $y[n] = y_1[n]$. Firstly, this identity implies that $f_{\mathrm{r}}()$ contains $f_1()$, since they both produce the same output signal $y[n]$, while the inputs and outputs of the former clearly form a superset of those of the latter. This, in turn, means that $x_1[n]$ is internal to $f_{\mathrm{r}}()$, because no outer part of the system may refer to it. It is then possible to identify an operator $f()$ that eliminates this input/output redundancy by safely stating $f_{\mathrm{r}}(x[n], y[n], x_1[n]) = (f(x[n], y[n]), x_1[n])$. Since $f_1()$ and $x_1[n]$ are both internal to $f()$, there necessarily needs to be a separated operator $x_1[n] = f_2(x[n], y[n])$, which lets $f()$ be defined in terms of the composition

$$\begin{aligned} y[n] &= f(x[n], y[n]) = f_1(x_1[n], y[n]) \\ &= f_1(f_2(x[n], y[n]), y[n]). \end{aligned} \tag{21}$$

When both $f_1()$ and $f_2()$ satisfy the requirements specified for $f()$ in Subsection III-A, it is possible to apply the described delay-free loop implementation method, first locally to the inner filter and then globally. Fig. 3 illustrates this scenario.

In this case, the inner filter can be implemented employing one of the solutions introduced before, and obviously without affecting its linear response. Therefore, for the outer loop, following an analogous reasoning to Subsection III-A, one gets

$$\begin{aligned} \widehat{C}(z) = &\frac{c_1 + H_{\mathrm{v},1}(z) c_2}{1 - H_{\mathrm{w},1}(z)} \frac{z^{-1}}{1 - z^{-1}} \\ &\left[\frac{\frac{1 - H_{\mathrm{w},1}(z)}{H_{\mathrm{ff}}(z)} - z^{-1} H_{\mathrm{fb}}(z) H_{\mathrm{v},1}(z) H_{\mathrm{w},2}(z)}{1 - H_{\mathrm{w},1}(z) - H_{\mathrm{v},1}(z) H_{\mathrm{w},2}(z)} - 1 \right], \end{aligned} \tag{22}$$

and

$$\begin{aligned} &\frac{1}{1 - H_{\mathrm{w},1}(z) - H_{\mathrm{v},1}(z) H_{\mathrm{w},2}(z)} \\ &= \frac{H_{\mathrm{ff}}(z) H_{\mathrm{in}}(z)}{1 - H_{\mathrm{w},1}(z) - z^{-1} H_{\mathrm{fb}}(z) H_{\mathrm{ff}}(z) H_{\mathrm{v},1}(z) H_{\mathrm{w},2}(z)}, \end{aligned} \tag{23}$$

which corresponds to (13) with

$$\sum_{i=0}^{A} a_i z^{-i} = \frac{L_2(z) M_1(z)\,(1 - N_1(z))}{1 - l_0}, \tag{24}$$

$$\begin{aligned} \sum_{i=1}^{D} d_i z^{-i} = &\left[N_2(z) + (1 - N_2(z)) \frac{N_1(z) + L_1(z)}{1 - l_0} \right] \\ &(1 - O_1(z)) + O_1(z), \end{aligned} \tag{25}$$

where $H_{\mathrm{v},1} = \frac{M_1(z)}{1 - O_1(z)}$, $H_{\mathrm{w},1} = \frac{l_0 + L_1(z)}{1 - N_1(z)}$, $H_{\mathrm{w},2} = \frac{L_2(z)}{1 - N_2(z)}$. This means that $H_{\mathrm{in}}(z)$, $H_{\mathrm{fb}}(z)$, and $H_{\mathrm{ff}}(z)$ can be determined with the same approach using coefficient values according to these last two equations. Note that the coefficients d_i depend on $L_1(z)$, and therefore they could be nonzero even if $H_{\mathrm{v},1}(z)$, $H_{\mathrm{v},2}(z)$, $H_{\mathrm{w},1}(z)$, and $H_{\mathrm{w},2}(z)$ were all FIR filters. This consideration justifies the use of the linear approximation outlined in Subsection III-A.

D. Remarks

The proposed method can be considered to be a wide generalization of Härmä's delay-free loop implementation technique [11], which essentially corresponds to the outlined FIR-only

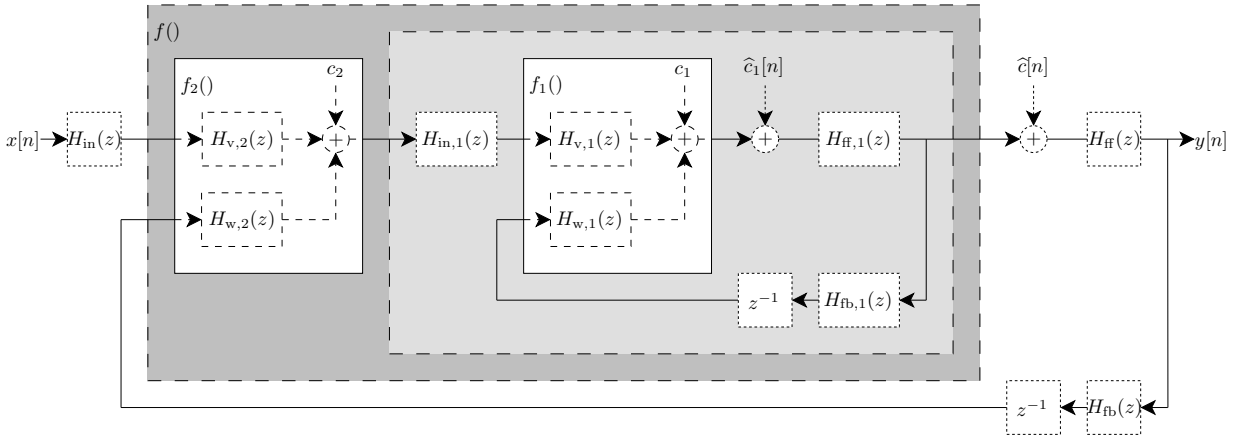

Fig. 3. Composition of two filters having delay-free loops. Components delimited by dashed lines are fictitious and represent either linear approximations around the given operating point (white background) or groups of other components (grey background), while those delimited by dotted lines are only present in the analogous computable implementation.

solution with $A = D = 0$, $r_0 = 1$, and $r_1 = 0$, applied to purely linear systems using the superposition principle. On the other hand, the proposed technique differs from other non-iterative delay-free implementation methods, such as the K-method [17] and its variants [18]–[20], in that it does not require any transformation of nonlinearities. Furthermore, it is the only technique that is not dependent upon a separation of instantaneous and historical components of signals.

However, the transformation of implicit filters using the proposed technique affects, in the general case, both their stability and global accuracy. These topics, while holding fundamental relevance, are not investigated in this study and are deferred to future investigations.

IV. Digital Implementation

Given the results enounced in Section III, the nonlinear circuit model described by (1) and (2) can be implemented by an infinite variety of non-iterative filters that preserve the linear response around the operating point. This section describes a subclass of such filters, for any number of stages N, obtained by applying minimum cost FIR-only solutions to delay-free loop problems.

A. Ladder Stages

The discrete-time ladder stage equation (5) can be linearly approximated around the operating point $\Delta V_{i-1,0} = 0, \Delta V_{i,0} = 0$ as

$$\begin{aligned}\Delta V_i[n] = \Delta V_i[n-1] + g(\Delta V_{i-1}[n] + \Delta V_{i-1}[n-1] \\ - \Delta V_i[n] - \Delta V_i[n-1]),\end{aligned} \tag{26}$$

which, according to the notation employed in Section III, can correspond to $A = 1$, $D = 1$, $a_0 = a_1 = -g$, and $d_1 = 1$. Applying (18) with $r_0 = 1$ leads to

$$p_0 = \frac{1}{1+g}, q_0 = 1 - g, r_1 = -g, \tag{27}$$

where g is defined by (6).

Equation (5) conveniently allows to interpret $\tanh\left(\frac{\Delta V_{i-1}[n]}{2V_\mathrm{T}}\right)$ as being the input of each stage, while this quantity is also required to be computed for the previous stage. Although the development in Section III suggests that nonlinearities should be placed as shown in Fig. 2(b), that is, in our case, on the feedback branch just before the summation with the input, one notices that moving such a nonlinearity to any place on the feedback branch does not affect the linear response around the operating point. Therefore, we can still perform a block diagram optimization described in both [7], [10] by which each stage only needs one nonlinearity. It consists in extracting two outputs, as shown in Fig. 4, so that the following stage gets its input from the bottom output, while the global output corresponds to the upper output of the last stage. This figure depicts both the original implicit ladder stage discretization (5), by disregarding components delimited by dotted lines, and the analogous explictly defined model, when taking them into account.

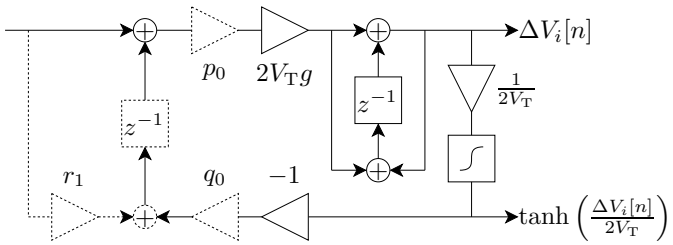

Fig. 4. Proposed digital ladder stage implementation. Components delimited by dotted lines are inserted to obtain the analogous computable implementation.

Following the same reasoning outlined in this subsection with (7) leads to an identical stage structure with the exception that the input signal would be $\tanh\left(\frac{V_\mathrm{u}[n]}{2V_\mathrm{T}}\right) = -\tanh\left(\frac{V_\mathrm{in}[n]+k\Delta V_N[n]}{2V_\mathrm{T}}\right)$.

B. Global Filter

As already anticipated at the beginning of Section III, the proposed model aims to allow the extraction of different frequency response modes by mixing the outputs of individual ladder stages, as described in [25]. Therefore the global

feedback path must be modeled in a way that preserves the linear relationship between each $\Delta V_i[n]$ stage output and the input signal around the operating point.

The linear transfer function of a single stage, according to (26), can be expressed by

$$\frac{\Delta V_i(z)}{\Delta V_{i-1}(z)} = \frac{g}{g+1}\frac{1+z^{-1}}{1+\frac{g-1}{g+1}z^{-1}}, \tag{28}$$

and therefore the transfer function between the i-th stage output and the sum of the input and the global feedback is given by

$$\begin{aligned}\frac{\Delta V_i(z)}{V_{\text{in}}(z)+k\Delta V_N(z)} &= -\left(\frac{\Delta V_i(z)}{\Delta V_{i-1}(z)}\right)^i \\ &= -\left(\frac{g}{g+1}\right)^i \frac{\sum_{j=0}^{i}\binom{i}{j}z^{-j}}{1+\sum_{j=1}^{i}\binom{i}{j}\left(\frac{g-1}{g+1}\right)^j z^{-j}}.\end{aligned} \tag{29}$$

In order to apply the composition method described in Subsection III-C, we define

$$H_{v,1}(z) = \frac{\Delta V_i(z)}{V_{\text{in}}(z)+k\Delta V_N(z)}, \tag{30}$$

$$H_{w,1}(z) = 0, \tag{31}$$

$$H_{w,2}(z) = k\left(\frac{\Delta V_i(z)}{\Delta V_{i-1}(z)}\right)^{N-i}, \tag{32}$$

which correspond to

$$M_1(z) = -\left(\frac{g}{g+1}\right)^i \sum_{m=0}^{i}\binom{i}{m}z^{-m}, \tag{33}$$

$$O_1(z) = -\sum_{m=1}^{i}\binom{i}{m}\left(\frac{g-1}{g+1}\right)^m z^{-m}, \tag{34}$$

$$L_2(z) = k\left(\frac{g}{g+1}\right)^{N-i}\sum_{m=0}^{N-i}\binom{N-i}{j}z^{-m}, \tag{35}$$

$$N_2(z) = -\sum_{m=1}^{N-i}\binom{N-i}{m}\left(\frac{g-1}{g+1}\right)^m z^{-m}, \tag{36}$$

$$l_0 = L_1(z) = N_1(z) = 0, \tag{37}$$

and eventually to

$$\sum_{m=0}^{A} a_m z^{-m} = -k\left(\frac{g}{g+1}\right)^N \sum_{m=0}^{N}\binom{N}{m}z^{-m}, \tag{38}$$

$$\sum_{m=1}^{D} d_m z^{-m} = -\sum_{m=1}^{N}\binom{N}{m}\left(\frac{g-1}{g+1}\right)^m z^{-m}, \tag{39}$$

which give $A = D = N$, $a_m = -k\binom{N}{m}\left(\frac{g}{g+1}\right)^N$, and $d_m = -\binom{N}{m}\left(\frac{g-1}{g+1}\right)^m$. Notice that these expressions do not depend on i, which implies that if the required compensation in the feedforward branch is applied before the digital ladder stages, the linear response between the individual outputs of each stage and the input signal is exact, and thus the extraction of different frequency response modes does not require extra components. The values of compensation coefficients can be obtained by using the corresponding FIR-only solution with $r_0 = 1$ as

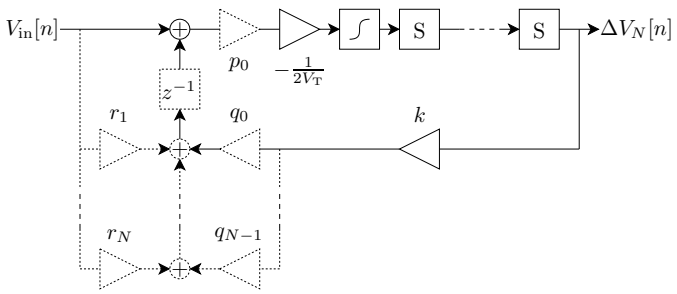

Fig. 5. Proposed global filter implementation. S denotes a ladder stage, while components delimited by dotted lines are inserted to obtain the analogous computable implementation.

$$p_0 = \frac{1}{1+k\left(\frac{g}{g+1}\right)^N}, \tag{40}$$

$$q_{m-1} = -\binom{N}{m}\left[k\left(\frac{g}{g+1}\right)^N + \left(\frac{g-1}{g+1}\right)^m\right], \tag{41}$$

$$r_m = -k\binom{N}{m}\left(\frac{g}{g+1}\right)^N, \tag{42}$$

where $m = 1, 2, 3, ...N$. A block diagram representation of the resulting filter is shown in Fig. 5, again overlaying the implicit global filter discretization and the proposed implementation.

V. Evaluation and Comparison

This section evaluates the fourth-order ($N = 4$) variant of the proposed implementation and compares it to the two best previous non-iterative nonlinear digital models [7], [10] and to a SPICE simulation [21] of the circuit in order to verify the validity and the usefulness of the results obtained so far. In order to perform a fair comparison, the proposed filter is parameterized in terms of the natural cut-off frequency $\widehat{f}_{\text{c}}$, as is already the case with previous emulators, but with bilinear pre-warping frequency $f_{\text{w}} = f_{\text{c}}$. Sound examples related to the tests performed in this section are available at the companion web page http://www.acoustics.hut.fi/go/ieee-taslp-2014-moog.

A. Linear Response

A first test was conducted to verify the preservation of the linear response of the filter around its operating point. The proposed implementation was configured with a resonance coefficient $k = 2$ and various cut-off frequency settings, and fed by a small-amplitude (0.01) impulse signal at a sample rate $f_{\text{s}} = 48\,\text{kHz}$, so that it operates mostly in its linear region. The output signals were then "normalized" by applying an inverse gain factor (i.e., $1/0.01 = 100$), and their magnitude responses were evaluated and compared to the corresponding theoretical linear magnitude responses. The same test was performed on Huovilainen's model [7] and on our previous model [10]. The results are shown in Fig. 6.

As expected, the proposed model exhibits perfect decoupling between cut-off frequency and resonance controls as

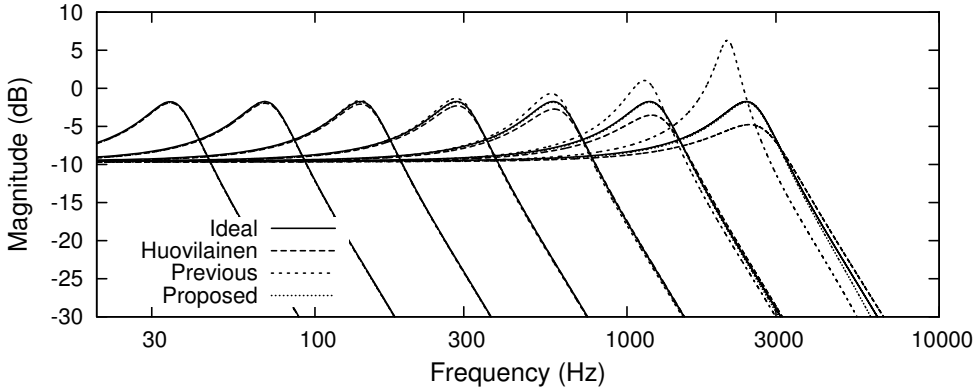

Fig. 6. Solid lines represent the "normalized" magnitude responses obtained by feeding the models with an impulse signal of amplitude 0.01 at a sample rate $f_\mathrm{s} = 48\,\mathrm{kHz}$, with $k = 2$, and $\widehat{f}_\mathrm{c} = 40.8\,\mathrm{Hz}$, $83.2\,\mathrm{Hz}$, $169.8\,\mathrm{Hz}$, $346.4\,\mathrm{Hz}$, $706.7\,\mathrm{Hz}$, $1441.7\,\mathrm{Hz}$, $2941.1\,\mathrm{Hz}$, $4200.8\,\mathrm{Hz}$. The corresponding theoretical linear magnitude responses are also shown, and they are almost indistinguishable from those generated by the proposed implementation.

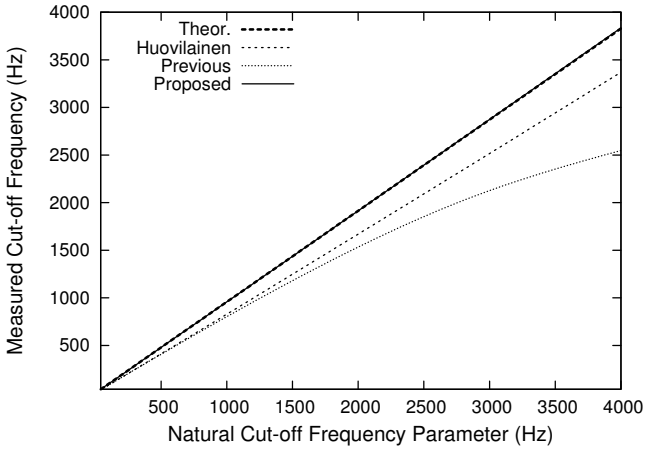

Fig. 7. Resulting cut-off frequency measured from the magnitude responses obtained by feeding the models with an impulse signal of amplitude 0.01 at a sample rate $f_\mathrm{s} = 48\,\mathrm{kHz}$, with $k = 2$ and different cut-off frequency parameter values. The lines representing the theoretical linear result and the proposed implementation are indistinguishable.

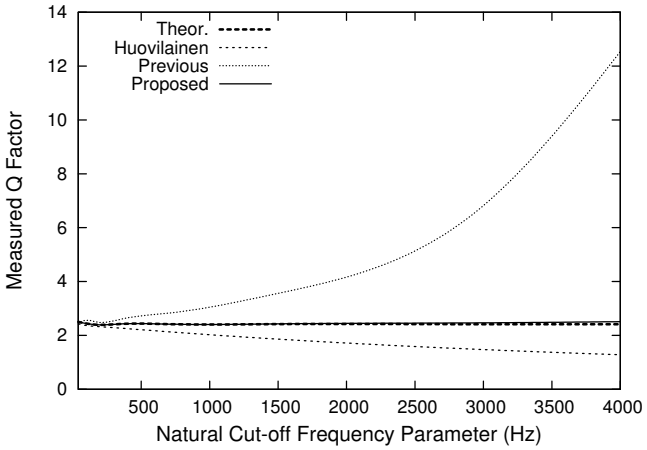

Fig. 8. Resulting Q factor measured from the magnitude responses obtained by feeding the models with an impulse signal of amplitude 0.01 at a sample rate $f_\mathrm{s} = 48\,\mathrm{kHz}$, with $k = 2$ and different cut-off frequency parameter values. The lines representing the theoretical linear result and the proposed implementation are mostly indistinguishable.

well as exact precision of cut-off frequency values, unlike the other two models. The only inconvenience is represented by the frequency warping effect at high frequencies due to the use of the bilinear transform in our derivation, but its effect is, in most cases, negligible w.r.t. the aliasing that these models inevitably introduce, or, in other words, it can be pragmatically overcome by oversampling, which would be, anyway, needed to reduce output noise.

Fig. 7 and Fig. 8 further illustrate these phenomena by comparing measured values of the resulting cut-off frequency and Q factor with the theoretical linear response, with $k = 2$ and different cut-off frequency parameter settings. In particular, the resulting cut-off frequency $\widetilde{f}_\mathrm{c}$ was measured by finding the frequency that corresponds to the maximum in the magnitude response, while the resulting Q factor was estimated as $Q \approx \widetilde{f}_\mathrm{c}/\Delta f$, where $\widetilde{f}_\mathrm{c}$ is the measured cut-off frequency and Δf is the half-power bandwidth. The outcome of this analysis is completely consistent with previous results.

B. Nonlinear Behavior

A second test was performed to evaluate the nonlinear behavior by means of *logsweep analysis* [26]. The system was fed with a 2-s long, logarithmically-swept sine signal of fixed amplitude 0.1 from $20\,\mathrm{Hz}$ to $100\,\mathrm{kHz}$ at a sample rate $f_\mathrm{s} = 384\,\mathrm{kHz}$, after which the output was convolved with the time-reversed and amplitude-weighted excitation signal, eventually obtaining an impulse reponse signal where the linear response and the individual harmonic distortion components are separated from each other in time. The model parameters used were $\widehat{f}_\mathrm{c} = 1\,\mathrm{kHz}$ and $k = 4$.

Fig. 9 depicts the resulting normalized harmonic spectra up to the 10^{th} harmonic for the three models and for a SPICE simulation of the circuit, hereby used as a reference. While all the models reasonably resemble the reference, the main differences occur around the cut-off frequency $1\,\mathrm{kHz}$. Unluckily, it is nontrivial to provide an objective measure, based on this analysis, of the diffformity from the ideal result due to both cut-off frequency shifting phenomena in the previous models

and frequency warping induced by the bilinear transform, but however, it is still possible to notice that both the previous and the proposed model generate significant high-order harmonic content around the cut-off frequency, similarly to the SPICE simulation, and unlike Huovilainen's model. Furthermore, it is possible to notice how the nonlinear saturation in each ladder stage affects the fundamental harmonic response by significantly reducing the resonant frequency and the amount of resonance.

By examining the output signal waveforms, as depicted in Fig. 10, this analysis reveals other interesting aspects of the behavior of both the original device and the digital models being discussed. Firstly, one immediately notices an amplitude increase when the instantaneous frequency of the input signal is about $300\,\mathrm{Hz}$, which corresponds to a substantial lack of high-order harmonic content, as visible in Fig. 9. This indicates that much of the high-order harmonic content, at least at low frequencies, is due to saturation effects. Then, Fig. 10(b) shows that the most relevant differences occur when the input signal has a low instantaneous frequency and that they are related to self-oscillation effects, thus revealing the nature of the high-order harmonic content around $1\,\mathrm{kHz}$. In particular, and in accordance with Fig. 9, our previous model generates excessive self-oscillation, while the proposed and, even more so, Huovilainen's model are lacking in this sense. At higher instantaneous frequencies of the input signal, the self-oscillating behavior of the device appears significantly reduced, and indeed the three models produce substantially identical results to each other and to the reference.

The amount of self-oscillation relative to the output signal amplitude decreases as the input signal level increases, and it is indeed possible to verify that the divergences between the models and the reference tend to be less evident in this case, thus further confirming the validity of this analysis. It is also worth mentioning that self-oscillation products are essentially independent of the cut-off frequency setting in the proposed model and the reference simulations, while they change in a way that resembles the Q factor deviation in both previous emulators.

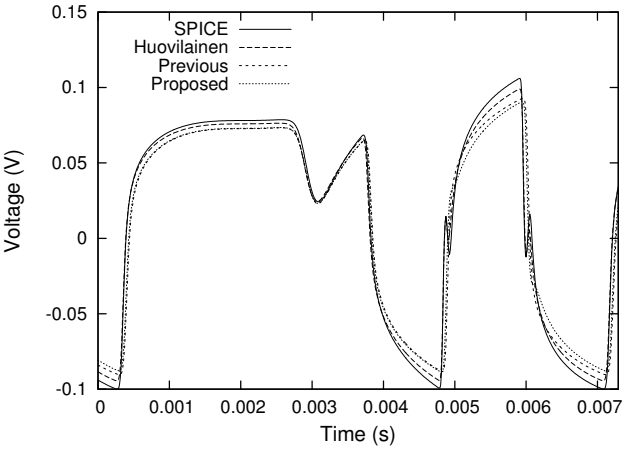

(a)

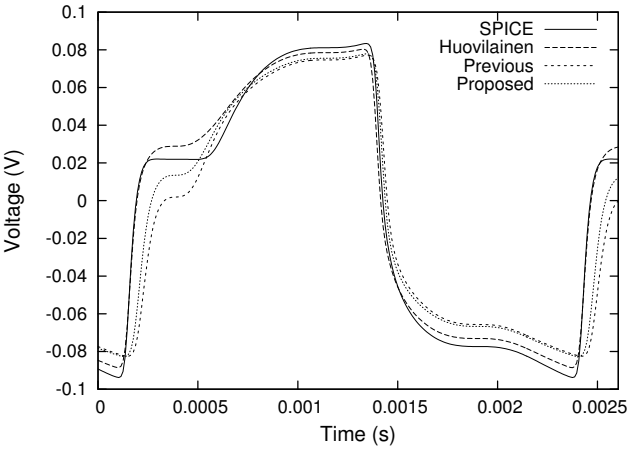

(b)

Fig. 11. Steady-state output signal waveforms obtained by exciting the models running at a sample rate $f_\mathrm{s} = 96\,\mathrm{kHz}$, and the corresponding SPICE simulations, with a 440-Hz sinusoidal input signal of amplitude 1, with $k = 4$, and a sinusoidal natural cut-off frequency signal $\widehat{f}_\mathrm{c}$ ranging from $20\,\mathrm{Hz}$ to $10\,\mathrm{kHz}$ with modulation frequency (a) $440/3\,\mathrm{Hz} \approx 146.67\,\mathrm{Hz}$, and (b) $440 \cdot 3\,\mathrm{Hz} = 1320\,\mathrm{Hz}$.

C. Time-Varying Behavior

The time-varying behavior of the three models was also tested by feeding them with a $440\,\mathrm{Hz}$ sinusoidal input signal of amplitude 1, with $f_\mathrm{s} = 96$ kHz, $k = 4$, and modulating the natural cut-off frequency parameter $\widehat{f}_\mathrm{c}$ as an audio-rate sinusoidal signal ranging from $20\,\mathrm{Hz}$ to $10\,\mathrm{kHz}$ with two different modulation frequencies, namely $440/3\,\mathrm{Hz} \approx 146.67\,\mathrm{Hz}$, and $440 \cdot 3\,\mathrm{Hz} = 1320\,\mathrm{Hz}$. These results were then compared to corresponding SPICE simulations, obtaining the steady-state output waveforms shown in Fig. 11. While the output signals obtained from Huovilainen's model more closely resemble the SPICE simulation results, such tests are not general enough to establish the superiority of any of the models, due to the dynamic nonlinear nature of the system. Nevertheless, the output waveforms closely resemble those obtained from SPICE simulations, indicating that all three models are capable of realistic audio-rate parametric control. One last test consisted in exciting the three emulators running at a sample rate $f_\mathrm{s} = 96\,\mathrm{kHz}$, $\widehat{f}_\mathrm{c} = 12\,\mathrm{kHz}$, and $k = 4$, with a 10-s long, 440-Hz sinusoidal input signal whose amplitude grew linearly from 0 to 1, which resulted in output signals with spectra containing only a few significant harmonic components and no perceivable noise, apart from early self-oscillation effects in our previous model at low input levels.

D. Stability

The time-varying stability of the proposed model with f_c-based parameterization can be theoretically evaluated for any N, assuming that the numerical representation of signals has infinite range and accuracy. Firstly, we notice that each digital ladder stage, depicted in Fig. 4, is preceded by a $\tanh()$ nonlinearity, which implies its input is limited to the range $[-1, 1]$. The bilinear-transformed integrator structure in each stage is necessarily stable, since it contains no time-varying parameter. Hence we only need to study the time-varying

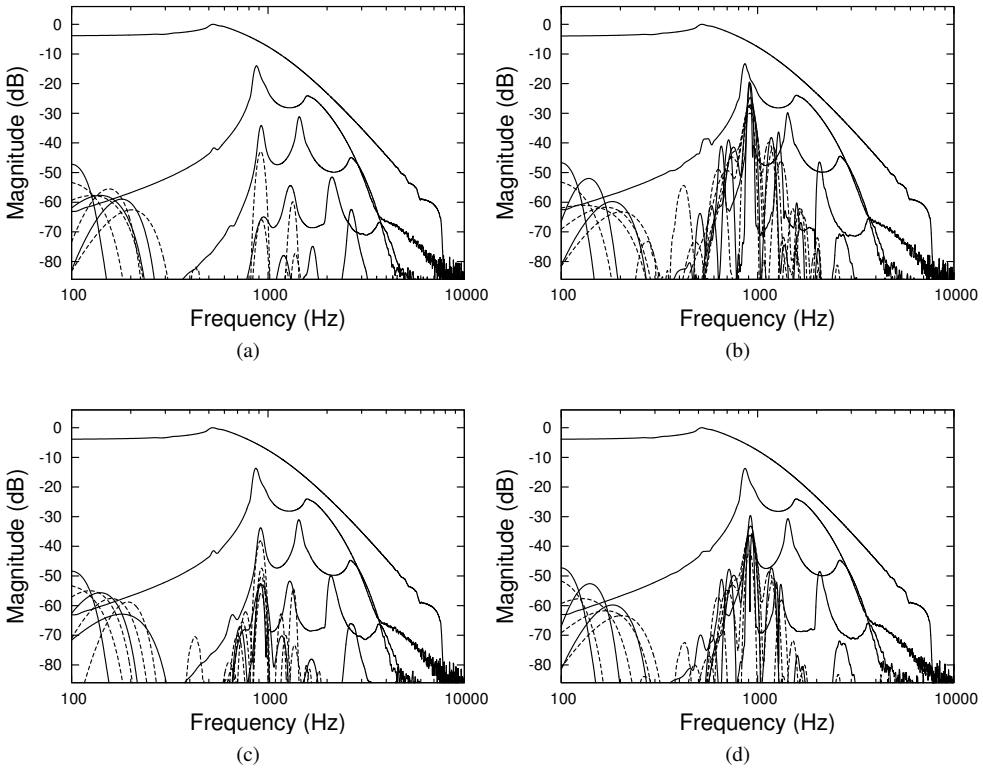

Fig. 9. Normalized harmonic spectra up to the 10th harmonic of the outputs obtained by exciting (a) Huovilainen's model [7], (b) our previous model [10], (c) the proposed model, and (d) the corresponding SPICE-simulated circuit with a 2-s long logarithmically swept sine signal of fixed amplitude 0.1 from 20 Hz to 100 kHz, with model parameters $\widehat{f}_\mathrm{c} = 1\,\mathrm{kHz}$ and $k = 4$. The operating sample rate for the three models is $f_\mathrm{s} = 384\,\mathrm{kHz}$. The fundamental and odd harmonic responses are represented by solid lines, even harmonic responses by dashed lines.

stability of its input, which can be expressed as

$$u_i[n] = 2V_\mathrm{T}\beta[n]\Bigg[\tanh\left(\frac{\Delta V_{i-1}[n]}{2V_\mathrm{T}}\right) - g[n-1]\tanh\left(\frac{\Delta V_{i-1}[n-1]}{2V_\mathrm{T}}\right) - \tanh\left(\frac{\Delta V_i[n-1]}{2V_\mathrm{T}}\right)\Bigg], \quad (43)$$

where $g[n] = \frac{\tan\left(\frac{\pi}{f_\mathrm{s}} f_\mathrm{c}[n]\right)}{\alpha(k[n])}$ and $\beta[n] = \frac{g[n]}{1+g[n]} = \frac{\tan\left(\frac{\pi}{f_\mathrm{s}} f_\mathrm{c}[n]\right)}{\alpha(k[n])+\tan\left(\frac{\pi}{f_\mathrm{s}} f_\mathrm{c}[n]\right)}$. Since this expression is symmetric for maxima and minima of $\Delta V_i[n]$ and $\Delta V_{i-1}[n]$, we can limit ourselves to studying

$$\begin{aligned}\max\left(|u_i[n]|\right) &= \max\left(u_i[n]\right) \\ &\leq 2V_\mathrm{T}\max\left(\beta[n]\right)\left[2 + \max\left(g[n]\right)\right] \\ &= 2V_\mathrm{T}[2 + \max\left(g[n]\right)],\end{aligned} \quad (44)$$

which is finite as long as $\max\left(g[n]\right)$ is finite, which is necessarily true when

$$0 \leq f_\mathrm{c}[n] < f_\mathrm{s}/2 \;\forall n. \quad (45)$$

The global feedback loop, as seen in Fig. 5, does not add other time-varying stability constraints since it essentially consists of a FIR structure whose output is limited by the first $\tanh()$ nonlinearity in the feedforward branch of the filter. This result indicates that the proposed filter structure is guaranteed to be stable to parameter variation as long as (45) is valid and the numerical representation has sufficient range and accuracy, also considering intermediate algorithm steps. In other words, the time-varying stability depends solely on condition (45), on the numerical representation employed, and on the relative order of operations in the actual implementation. Note that this analysis also reveals that the value of k does not play any role in the stability of the proposed model, and hence it can be arbitrarily large within the limits imposed by numerical range and accuracy.

In practical terms, however, finite wordlength undermines the accuracy of ladder stage structures, leading the simulation to states that are highly inconsistent with the original system. We have empirically verified, by feeding the model with white noise input and audio-rate control signals, and employing both single- and double-precision IEEE 754-2008 floating point numerical representations, that the filter always produces coherent results as long as $f_\mathrm{c} \leq f_\mathrm{s}/8$ is enforced, while no constraints need to be applied to k.

E. Computational Cost

The computational cost, in the general case, preserving $\Delta V_\mathrm{i}[n]$ stage outputs, and excluding the computation of filter coefficients, consists of $N + 1$ hyperbolic tangents, $6N + 2$ multiplications, $6N$ additions, and $3N$ unit delays. In the case $N = 4$ this means 5 hyperbolic tangents, 26 multiplications, 24

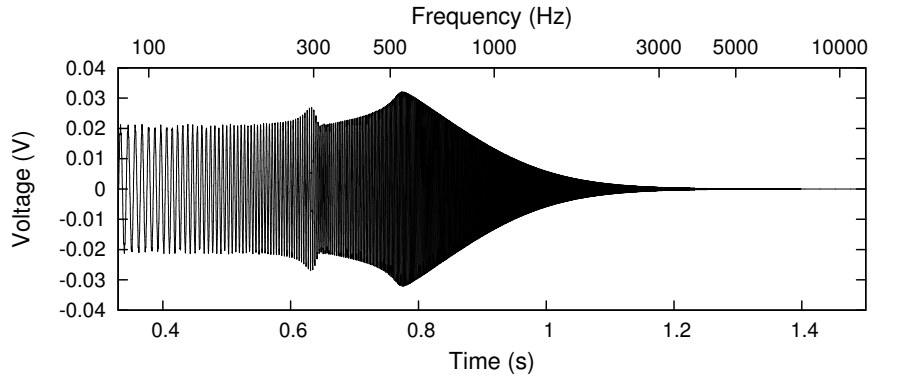

(a)

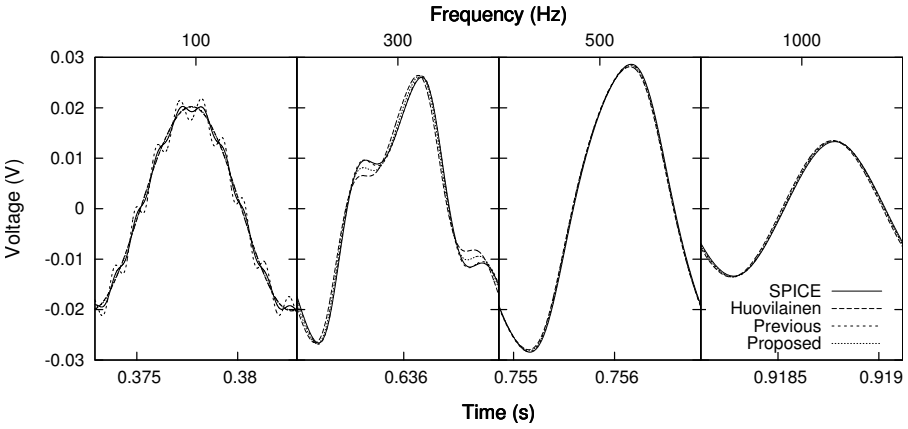

(b)

Fig. 10. Output signal waveforms corresponding to a 2-s long logarithmically-swept sine input signal of fixed amplitude 0.1 from 20 Hz to 100 kHz, with parameters $\widehat{f}_{\mathrm{c}} = 1\,\mathrm{kHz}$ and $k = 4$. (a) A large portion of the output obtained through the SPICE simulation. (b) Comparison of the output signals generated by the three models running at a sample rate $f_{\mathrm{s}} = 384\,\mathrm{kHz}$ with the SPICE simulation results around the time instants corresponding to the instantaneous frequencies of the input signal 100 Hz, 300 Hz, 500 Hz, and 1000 Hz.

additions, and 12 unit delays, thus resulting more in a greater cost than both Huovilainen's model (5 hyperbolic tangents, 10 multiplications, 9 additions, and 9 unit delays) and our previous model (5 hyperbolic tangents, 10 multiplications, 13 additions, and 9 unit delays). However, in all three cases, the computational load is clearly dominated by the evaluation of hyperbolic tangents, leading to comparable overall performance.

It is also worth noticing that the number of operations grows linearly with the number of stages N, and that it may be possible to obtain better CPU performance, at the expense of accuracy, by adopting common approximation techniques for the computation of hyperbolic tangents (e.g., polynomial approximations, Padé approximants, lookup tables), or by selectively removing nonlinearities from single stages as sketched in [25], potentially at the expense of some time-varying stability.

VI. Conclusion

This paper introduced a novel and general technique to implement delay-free loops non-iteratively in nonlinear filters in such a way that the linear response around a chosen operating point is preserved, the filter topology remains mostly unaffected, and no transformation of nonlinearities has to be performed.

This technique was then applied to obtain a digital implementation of the generalized Moog ladder filter presented in [6] for any number of ladder stages. The fourth-order variant of the proposed model was compared to its predecessors [7], [10] and was found to outperform them in terms of linear response, and especially w.r.t. precision and coupling of filter parameters, while retaining accurate nonlinear behavior. Moreover, it allows the extraction of different frequency-response modes, as outlined in [25], without the addition of extra components, it exhibits excellent time-varying stability properties, and only requires a relatively modest increase in computational load.

Supplementary material to this paper, including sound examples, can be accessed at http://www.acoustics.hut.fi/go/ieee-taslp-2014-moog.

References

[1] R. A. Moog, "A voltage-controlled low-pass high-pass filter for audio signal processing," in *Proc. 17th AES Convention*, New York, USA, October 1965.

[2] ——, "Electronic high-pass and low-pass filters employing the base to emitter diode resistance of bipolar transistors," October 1969, U.S. Patent 3,475,623.

[3] D. Rossum, "Making digital filters sound analog," in *Proc. Intl. Computer Music Conf. (ICMC 1992)*, San Jose, CA, USA, October 1992, pp. 30–34.

[4] V. Välimäki, F. Fontana, J. O. Smith, and U. Zölzer, "Introduction to the special issue on virtual analog audio effects and musical instruments," *IEEE Trans. Audio, Speech and Lang. Process.*, vol. 18, no. 4, pp. 713–714, May 2010.
[5] V. Välimäki, S. Bilbao, J. O. Smith, J. S. Abel, J. Pakarinen, and D. Berners, "Virtual analog effects," in *DAFX: Digital Audio Effects, Second Edition*, U. Zölzer, Ed. Chichester, UK: Wiley, 2011, pp. 473–522.
[6] S. D'Angelo and V. Välimäki, "Generalized Moog ladder filter: Part I – linear analysis and parameterization," *paper submitted for publication*.
[7] A. Huovilainen, "Non-linear digital implementation of the Moog ladder filter," in *Proc. 7th Intl. Conf. Digital Audio Effects (DAFx-04)*, Naples, Italy, October 2004, pp. 61–64.
[8] F. Fontana, "Preserving the structure of the Moog VCF in the digital domain," in *Proc. Intl. Computer Music Conf. (ICMC 2007)*, Copenhagen, Denmark, August 2007, pp. 291–294.
[9] T. Hélie, "Volterra series and state transformation for real-time simulations of audio circuits including saturations: Application to the Moog ladder filter," *IEEE Trans. Audio, Speech and Lang. Process.*, vol. 18, no. 4, pp. 747–759, May 2010.
[10] S. D'Angelo and V. Välimäki, "An improved virtual analog model of the Moog ladder filter," in *Proc. Intl. Conf. on Acoustics, Speech, and Signal Process. (ICASSP 2013)*, Vancouver, Canada, May 2013, pp. 729–733.
[11] A. Härmä, "Implementation of recursive filters having delay free loops," in *Proc. Intl. Conf. on Acoustics, Speech, and Signal Process. (ICASSP 1998)*, vol. 3, Seattle, USA, May 1998, pp. 1261–1264.
[12] F. Fontana, "Computation of linear filter networks containing delay-free loops, with an application to the waveguide mesh," *IEEE Trans. Speech and Audio Process.*, vol. 11, no. 6, pp. 774–782, November 2003.
[13] F. Fontana, F. Avanzini, and D. Rocchesso, "Computation of nonlinear filter networks containing delay-free paths," in *Proc. 7th Intl. Conf. Digital Audio Effects (DAFx-04)*, October 2004, pp. 113–118.
[14] F. Avanzini, F. Fontana, and D. Rocchesso, "Efficient computation of nonlinear filter networks with delay-free loops and applications to physically-based sound models," in *Proc. 4th Intl. Workshop on Multidim. Systems (NDS 2005)*, Wuppertal, Germany, July 2005, pp. 110–115.
[15] F. Fontana and F. Avanzini, "Computation of delay-free nonlinear digital filter networks: Application to chaotic circuits and intracellular signal transduction," *IEEE Trans. Signal Process.*, vol. 56, no. 10, pp. 4703–4715, September 2008.
[16] A. Falaize-Skrzek and T. Hélie, "Simulation of an analog circuit of a wah pedal: A port-hamiltonian approach," in *Proc. 135th AES Convention*, New York, USA, October 2013.
[17] G. Borin, G. De Poli, and D. Rocchesso, "Elimination of delay-free loops in discrete-time models of nonlinear acoustic systems," *IEEE Trans. Audio, Speech and Lang. Process.*, vol. 8, no. 5, pp. 597–605, September 2000.
[18] D. Yeh, J. Abel, and J. Smith, "Automated physical modeling of nonlinear audio circuits for real-time audio effects–part I: Theoretical development," *IEEE Trans. Audio, Speech and Lang. Process.*, vol. 18, no. 4, pp. 728–737, April 2010.
[19] D. Yeh, "Automated physical modeling of nonlinear audio circuits for real-time audio effects–part II: BJT and vacuum tube examples," *IEEE Trans. Audio, Speech, and Lang. Process.*, vol. 20, no. 4, pp. 1207–1216, May 2012.
[20] K. Dempwolf, M. Holters, and U. Zölzer, "Discretization of parametric analog circuits for real-time simulations," in *Proc. 13th Intl. Conf. Digital Audio Effects (DAFx-10)*, Graz, Austria, September 2010.
[21] J. M. Rabaey, "The Spice home page," http://bwrcs.eecs.berkeley.edu/Classes/IcBook/SPICE/, accessed 04 December 2013.
[22] M. Civolani and F. Fontana, "A nonlinear digital model of the EMS VCS3 voltage-controlled filter," in *Proc. 11th Intl. Conf. Digital Audio Effects (DAFx-08)*, Espoo, Finland, September 2008, pp. 35–42.
[23] F. Fontana and M. Civolani, "Modeling of the EMS VCS3 voltage-controlled filter as a nonlinear filter network," *IEEE Trans. Audio, Speech, and Lang. Process.*, vol. 18, no. 4, pp. 760–772, May 2010.
[24] S. Zambon and F. Fontana, "Efficient polynomial implementation of the EMS VCS3 filter model," in *Proc. 14th Intl. Conf. Digital Audio Effects (DAFx-11)*, Paris, France, September 2011, pp. 287–290.
[25] V. Välimäki and A. Huovilainen, "Oscillator and filter algorithms for virtual analog synthesis," *Comput. Music J.*, vol. 30, no. 2, pp. 19–31, June 2006.
[26] A. Farina, "Simultaneous measurement of impulse response and distortion with a swept-sine technique," in *Proc. 108th AES Convention*, Paris, France, February 2000.

Stefano D'Angelo was born in Vallo della Lucania, Italy, in 1987. He received the M.S. degree in Computer Engineering from Politecnico di Torino, Turin, Italy, in 2010. In 2009-2010, he was an Erasmus exchange student at the Helsinki University of Technology, Espoo, Finland. He is currently a doctoral student at the Department of Signal Processing and Acoustics at the Aalto University, School of Electrical Engineering, Espoo, Finland. His main research interests are audio programming languages and digital emulation of electric audio circuits.

Vesa Välimäki (S90–M92–SM99) received the M.S. (Tech.), the Licentiate of Science in Technology, and the Doctor of Science in Technology degrees, all in electrical engineering, from the Helsinki University of Technology (TKK), Espoo, Finland, in 1992, 1994, and 1995, respectively.

He was a Postdoctoral Research Fellow at the University of Westminster, London, UK, in 1996. In 1997-2001, he was a Senior Assistant (cf. Assistant Professor) at the TKK Laboratory of Acoustics and Audio Signal Processing, Espoo, Finland. From 1998 to 2001, he was on leave as a Postdoctoral Researcher under a grant from the Academy of Finland. In 2001-2002, he was Professor of signal processing at the Pori unit of the Tampere University of Technology, Pori, Finland. He was appointed Docent in signal processing at the Pori unit of the Tampere University of Technology in 2003. In 2006-2007, he was the Head of the TKK Laboratory of Acoustics and Audio Signal Processing. He is currently Professor in the Department of Signal Processing and Acoustics, Aalto University, Espoo, Finland. In 2008-2009, he was on sabbatical as a Visiting Scholar at the Center for Computer Research in Music and Acoustics (CCRMA), Stanford University, Stanford, CA. His research interests include audio effects processing, digital filtering, sound synthesis, and acoustics of musical instruments.

Prof. Välimäki is a senior member of the IEEE, a fellow of the Audio Engineering Society, a member of the Finnish Musicological Society, and a life member of the Acoustical Society of Finland. In 2000-2001, he was Secretary of the IEEE Finland Section. He was President of the Finnish Musicological Society in 2003-2005. In 2008, he was the Chairman of DAFx-08, the 11th International Conference on Digital Audio Effects (Espoo, Finland). He has served as an Associate Editor of the IEEE TRANSACTIONS ON AUDIO, SPEECH AND LANGUAGE PROCESSING and of the IEEE SIGNAL PROCESSING LETTERS. He was the Lead Guest Editor of a special issue of the IEEE SIGNAL PROCESSING MAGAZINE in 2007 and of a special issue of the IEEE TRANSACTIONS ON AUDIO, SPEECH AND LANGUAGE PROCESSING in 2010. He is a member of the Audio and Acoustic Signal Processing Technical Committee of the IEEE Signal Processing Society.